Crystal structure, Hirshfeld surfaces and DFT computation of NLO active (2E)-2-(ethoxycarbonyl)-3-[(1-methoxy-1-oxo-3-phenylpropan-2-yl)amino] prop-2-enoic acid

Venkatesan, Perumal

2016-01-15

Venkatesan , P , Thamotharan , S , Ilangovan , A , Liang , H & Sundius , T 2016 , ' Crystal structure, Hirshfeld surfaces and DFT computation of NLO active (2E)-2-(ethoxycarbonyl)-3-[(1-methoxy-1-oxo-3-phenylpropan-2-yl)amino] prop-2-enoic acid ' , Spectrochimica Acta Part A: Molecular and Biomolecular Spectroscopy , vol. 153 , pp. 625-636 . https://doi.org/10.1016/j.saa.2015.09.002

http://hdl.handle.net/10138/173639
https://doi.org/10.1016/j.saa.2015.09.002

acceptedVersion

Elsevier Editorial System(tm) for
Spectrochimica Acta Part A: Molecular and Biomolecular Spectroscopy
Manuscript Draft

Manuscript Number: SAA-D-14-01884R1

Title: Crystal structure, Hirshfeld surfaces and DFT computation of NLO active (2E)-2-(ethoxycarbonyl)-3-[(1-methoxy-1-oxo-3-phenylpropan-2-yl)amino] prop-2-enoic acid

Article Type: Full Length Article

Keywords: Second Harmonic Generation; Malonic acid half-ester; Hirshfeld surface; polarizability; first order hyperpolarizability; PIXEL.

Corresponding Author: Prof. Andivelu Ilangovan, M.Sc., Ph.D.,

Corresponding Author's Institution: Bharathidasn University

First Author: Venkatesan Perumal

Order of Authors: Venkatesan Perumal ; Thamotharan Subbiah; Andivelu Ilangovan, M.Sc., Ph.D.,; Hongze Liang ; Sundius Tom, Ph.D.,

Abstract: Nonlinear optical (NLO) activity of the compound (2E)-2-(ethoxycarbonyl)-3-[(1-methoxy-1-oxo-3-phenylpropan-2-yl)amino] prop-2-enoic acid is investigated experimentally and theoretically using X-ray crystallography and quantum chemical calculations. The NLO activity is confirmed by both powder Second Harmonic Generation (SHG) experiment and first hyper polarizability calculation. The title compound displays 8 fold excess of SHG activity when compared with the standard compound KDP. The gas phase geometry optimization and vibrational frequencies calculations are performed using density functional theory (DFT) incorporated in B3LYP with 6-311G++(d,p) basis set. The title compound crystallizes in non-centrosymmetric space group P21. Moreover, the crystal structure is primarily stabilized through intramolecular N-H…O and O-H…O hydrogen bonds and intermolecular C-H…O and C-H…π interactions. These intermolecular interactions are analyzed and quantified using Hirshfeld surface analysis and PIXEL method. The detailed vibrational assignments are performed on the basis of the potential energy distributions (PED) of the vibrational modes.

07th August 2014

To
The Editor
Spectrochimica Acta Part A: Molecular and Biomolecular Spectroscopy

Dear Editor,

As suggested, we have revised our manuscript carefully.

We have enclosed the revised manuscript entitled **Crystal structure, Hirshfeld surfaces and DFT computation of NLO active (2*E*)-2- (ethoxycarbonyl)-3-[(1-methoxy-1-oxo-3-phenylpropan-2-yl)amino]prop-2-enoic acid** for possible publication in the Spectrochimica Acta Part A: Molecular and Biomolecular Spectroscopy. The manuscript examines the NLO activity of the compound **(2*E*)-2- (ethoxycarbonyl)-3-[(1-methoxy-1-oxo-3-phenylpropan-2-yl)amino]prop-2-enoic acid** using experimental and theoretical calculations. The NLO active title compound crystallizes in non-centrosymmetric space group ($P2_1$). We found that the compound discussed in this paper displays 8 fold excess of second harmonic generation efficiency when compared with standard KDP. The crystal structure of the compound is also discussed. Potential intermolecular contacts present in the crystal structures are identified using Hirshfeld surface analysis and the energetics of the molecular pairs which held together by various intermolecular contacts are presented. Interestingly, the strength of the intermolecular C–H…π interaction is stronger than some of the intermolecular C–H…O interactions. The frontier molecular orbital energy, dipole moment, polarizability and first order hyperpolarizability are calculated for the title compound using DFT computation.

The manuscript presents original work and has not been submitted elsewhere for publication. We have also included names of four experts as potential reviewers.

Thank you for your consideration,

Sincerely,

Andivelu Ilangovan

Dear Professor James R. Durig,

Thank you very much for extending time to revise our manuscript based on reviewer-2 comments. As suggested by the reviewer-2, we have now included the vibrational assignments of the title molecule and also included the experimental and theoretical spectrogram of FT-IR and FT-Raman. The appropriate references are cited in the text and arranged them in the reference section as well.

We have included Prof. Tom Sundius as an author in the revised manuscript. He has involved in the vibrational assignments of the title molecule. We are hoping that you will accept the changes that we have made.

We would like to thank you and the anonymous reviewers for their comments.

Yours sincerely,

AndiveluIlangovan

Reviewer #2: In the manuscript titled 'Crystal structure, Hirshfeld surfaces and DFT computation of NLO active (2E)-2-(ethoxycarbonyl)-3-[(1-methoxy-1-oxo-3-phenylpropan-2-yl)amino] prop-2-enoic acid' authors mainly reported theoretical study of the molecule and it has very limited spectroscopy. Hence this manuscript give very limited contribution in the field of spectroscopy. However authors can improve the manuscript by reporting the infrared, Raman and vibrational assignment of the molecule. I leave final decision to the editor whether to accept or reject this manuscript.

GRAPHICAL ABSTRACT

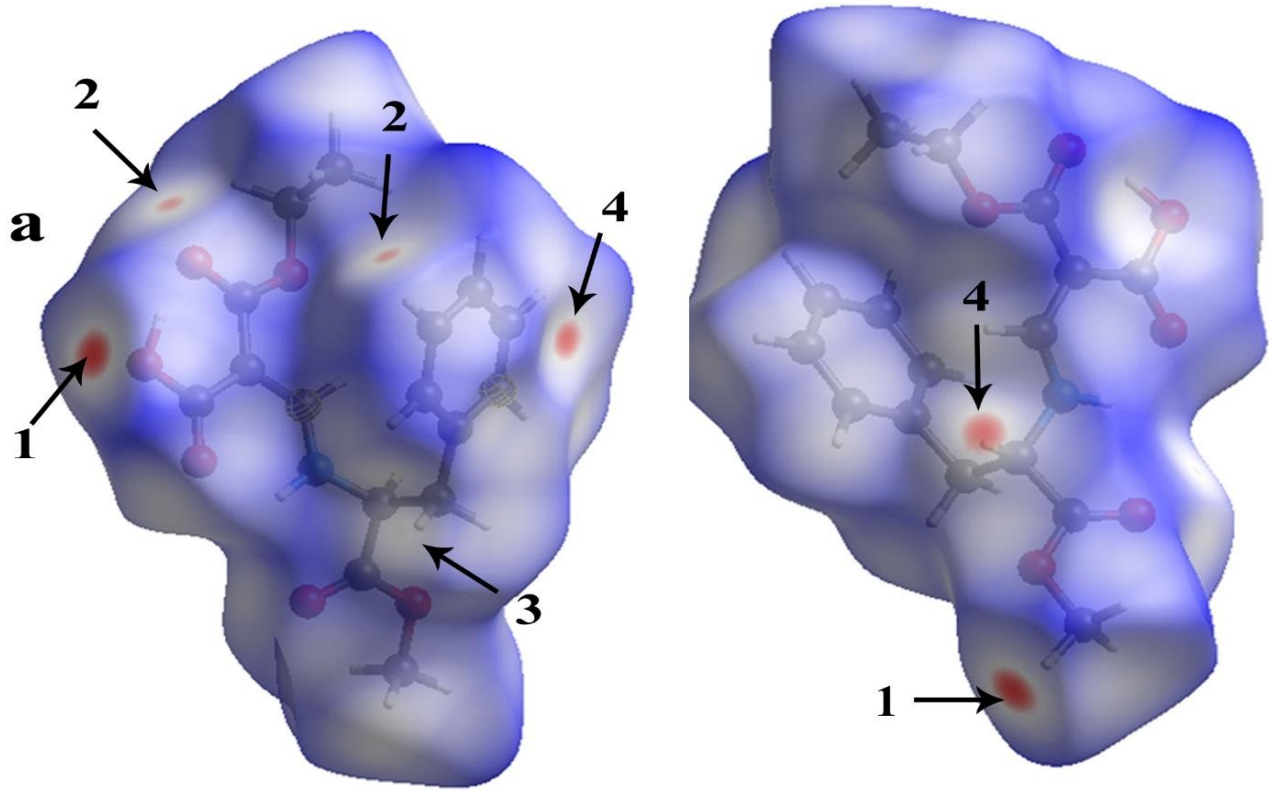

HIGHLIGHTS

- Non linear optical active (2*E*)-2- (ethoxycarbonyl)-3-[(1-methoxy-1-oxo-3-phenylpropan-2-yl)amino]prop-2-enoic acidis synthesized and single crystals are grown suitable for X-ray diffraction studies.
- The compound crystallizes in non-centrosymmetric space group $P2_1$.
- The SHG efficiency of the compound displays 8 fold excess when compared with standard KDP.
- Intermolecular interactions are analysed using Hirshfeld surfaces.
- The energetics of molecular pairs isestimated using PIXEL method.
- Mulliken atomic charges, polarizability, hyperpolarizability and molecular electrostatic potential are calculated using DFT computation.

Crystal structure, Hirshfeld surfaces and DFT computation of NLO active (2*E*)-2-(ethoxycarbonyl)-3-[(1-methoxy-1-oxo-3-phenylpropan-2-yl)amino] prop-2-enoic acid

Perumal Venkatesan,[a] Subbiah Thamotharan,[b*] Andivelu Ilangovan,[a*] Hongze Liang[c] and Tom Sundius[d]

[a] School of Chemistry, Bharathidasan University, Tiruchirappalli 620 024, Tamilnadu, India. Fax +91- 431 2407045 /2412750; Tel: +91-98654 36093; Email: ilangovanbdu@yahoo.com

[b] Department of Bioinformatics, School of Chemical and Biotechnology, SASTRA University, Thanjavur 613 401, Tamilnadu, India. Fax +91- 4362264120; Tel: +91-4362264101; Email: thamu@scbt.sastra.edu

[c] The State Key Laboratory Base of Novel Functional Materials and Preparation Science, Faculty of Materials and Chemical Engineering, Ninbgo University, 315211,People's Republic of China.

[d] Department of Physics, University of Helsinki, P.O. Box 64, FIN-00014 Helsinki, Finland.

Abstract

Nonlinear optical (NLO) activity of the compound (2*E*)-2-(ethoxycarbonyl)-3-[(1-methoxy-1-oxo-3-phenylpropan-2-yl)amino] prop-2-enoic acid is investigated experimentally and theoretically using X-ray crystallography and quantum chemical calculations. The NLO activity is confirmed by both powder Second Harmonic Generation (SHG) experiment and first hyper polarizability calculation. The title compound displays 8 fold excess of SHG activity when compared with the standard compound KDP. The gas phase geometry optimization and vibrational frequencies calculations are performed using density functional theory (DFT) incorporated in B3LYP with 6–311G++(d,p) basis set. The title compound crystallizes in non–centrosymmetric space group $P2_1$. Moreover, the crystal structure is primarily stabilized through intramolecular N–H…O and O–H…O hydrogen bonds and intermolecular C–H…O and C–H…π interactions. These intermolecular interactions are analyzed and quantified using Hirshfeld surface analysis and PIXEL method. The detailed vibrational assignments are performed on the basis of the potential energy distributions (PED) of the vibrational modes.

Keyword: Second Harmonic Generation,Malonic acid half–ester,Hirshfeld surface, polarizability, first order hyperpolarizability, PIXEL.

Introduction

Second Harmonic Generation (SHG) is usually observed in non–centrosymmetric materials. Structures of the majority of the NLO materials contain electron donor-acceptor groups connected through π–conjugation bridge [1,2]. Increasing the length of the π–conjugation enhances the molecular hyperpolarizability (β) and favors large second order nonlinear optical response [3]. However, the electrostatic interaction induces the molecules to arrange and align themselves in centrosymmetric fashion in the macroscopic level or in the solid state. Only about 25% of all achiral molecules crystallize in acentric space groups [4,5], among which only a few organic dipolar chromophoric molecules are found to arrange in acentric manner in the solid state. In a centrosymmetric system, the overall dipole moment gets cancelled and the SHG activity of the individual molecules gets nullified. It is a prerequisite for the development of new second–order NLO materialswhich crystallize in non–centrosymmetric environments. Various approaches are used such as controlling the molecular self–assembly through hydrogen bonding and weak van der Waals interactions and introduction of chiral center [6] or an octupole [7] in the molecule to achieve acentric nature in the crystalline material.

It is well known that the chiral amino acids and their complexes are promising materials for NLO applications [8–13]. Among them, *L*–phenylalanine, one of the hydrophobic aromatic amino acids, shows SHG efficiency of about one-third of the standard compound KDP [13]. Similarly, its derivatives also show SHG activity [14–23]. Based on this, it is envisaged that introduction of methylene malonic acid monoethyl ester group on amino group of phenylalanine may provide push pull type environment in addition to the chiral environment. *N*–Aminomethylene malonic acid possesses acid and ester group at geminal position and an amine group at vicinal position of the double bond may provide push pull environment and the presence of chiral carbon atom in the phenylalanine moiety helps to form a non–centrosymmetric crystal. Hence the title compound is expected to show good SHG activity. This activity is measured and confirmed experimentally.

Malonic acid half–esters, which falls under the class of geminal half–ester finds extensive applications as important intermediates in the synthesis of natural products such as virantmycin [24], amino acids [25], β–hydroxy esters or β–amino esters [26] and in the synthesis of tri carbonyl compounds [27]. The synthesis of functionalized malonic acid half–ester derivatives has been reported earlier by our group [28].

Hirshfeld surface diagram [29,30] and decomposed 2D fingerprint plots [31,32] have proven to be a simple visualization tool for the analysis of intermolecular interactions. The crystal structure of the title compound is mainly stabilized by intermolecular C–H…O/π interactions in addition to intramolecular O–H…O and N–H…O hydrogen bonds. These intermolecular interactions have been quantified in terms of breakdown of crystal structure into molecular pairs which are interconnected by various intermolecular interactions using PIXEL method [33–35]. Here, we report experimental and theoretical characterizations of an NLO active title compound(2*E*)-2-(ethoxycarbonyl)-3-[(1-methoxy-1-oxo-3-phenylpropan-2-yl)amino] prop-2-enoic acid.

.

Experimental

Synthesis of (2*E*)-2-(ethoxycarbonyl)-3-[(1-methoxy-1-oxo-3-phenylpropan-2-yl)amino] prop-2-enoic acid

The title compound was prepared by $BF_3.OEt_2$ mediated hydrolysis of germinal diester (Scheme 1) as reported earlier [28]. To a solution of diethyl {[(1-methoxy-1-oxo-3-phenylpropan-2-yl)amino]methylidene}propanedioate (1.0 equiv.) in $CHCl_3$ (3x w/v), $BF_3.OEt_2$ (1.0 equiv.) was added and stirred at 296 K. Completion of the reaction was determined by TLC. The reaction mixture was quenched with water (1x w/v) and extracted with chloroform (3x10 mL). The combined organic layer was dried (anhyd. Na_2SO_4) and evaporated in rotary evaporator under vacuum. The crude product obtained was passed through a short silica gel column using a hexane and ethyl acetate mixture (8:2, v/v) as eluent to obtain as a yellow solid (mp: 82 °C, 0.80 g, yield 82 %).The title compound recrystallized from ethanol by slow evaporation method. ^{1}H–NMR (400 MHz, $CDCl_3$) δ: 1.24 (t, J = 6.8 Hz, 3H), 3.02-3.08 (m, 1H), 3.29-3.33 (m, 1H), 3.80 (s,

3H), 4.10-4.26 (m, 3H), 7.16-7.18 (m, 2H), 7.25-7.35 (m, 3H), 10.15 (t, *J* = 9.6 Hz, 1H), 12.78 (brs, 1H); ^{13}C–NMR (100 MHz, $CDCl_3$) *δ*:14.1, 39.6, 52.9, 60.9 63.5, 87.8, 127.5, 128.9, 129.3, 134.7, 157.8, 169.6, 169.7, 170.5. The FT-IR spectrum of the title compound was recorded in the frequency region 4000–400 cm^{-1} on a Perkin Elmer-Spectrum one spectrometer using KBr pellet technique. The FT-Raman spectrum of the title compound was recorded using 1064 nm line of Nd:YAG laser as excitation wavelength in the region 4000–3 cm^{-1} on a Bruker RFS-27 FT-Raman spectrometer.The spectral data for the title compound is given in the supplementary information section. The NMR spectral data for the title compound is comparable with the data already reported [28].

Single crystal x-ray diffraction

A single crystal suitable for X–ray diffraction study was chosen carefully. The X–ray intensity data were collected at room temperature (296 K) with Bruker SMART APEX–II diffractometer using graphite monochromatic *MoKα* radiation (λ = 0.71073 Å). The crystal structure of the title compound was solved by SIR92 [36] and all the non-hydrogen atoms were refined anisotropically using the SHELXL–97 program [37]. The positions of amine and hydroxy H atoms were located from a difference Fourier map. The hydroxy (O–H) distance was restrained to 0.84(2)Å using DFIX option implemented in SHELXL program. The remaining H atoms were placed in idealized geometrical positions and constrained to ride on their parent atoms. The thermal ellipsoidal and crystal packing figures were produced using the programs PLATON [38] and MERCURY [39] respectively. CCDC 832624 contains the supplementary crystallographic data for this paper. These data can be obtained free of charge from The Cambridge Crystallographic Data Centre via www.ccdc.cam.ac.uk/data_request/cif.

Computational details

The gas phase geometry optimization was carried out with 6–311++G(d,p) basis set using Becke's three parameter exact exchange functional (B3) [40] with gradient-corrected correlation functional of Lee–Yang–Parr (LYP) of DFT [41,42] . The crystal structure of the title compound was taken as the starting structure for the gas phase geometry optimization. The vibrational frequencies were calculated at the same level of theory to assess the stationary point. No imaginary frequency was observed for the optimized structure. The polarizabilities and

hyperpolarizabilities were calculated from the DFT optimized structure using finite field approach. All the computations were performed using the Jaguar module implemented in Schrödinger suite 2013 [43]. The band gap energy (highest occupied molecular orbital (HOMO) –lowest unoccupied molecular orbital (LUMO)and molecular electrostatic potential map diagrams were produced using themaestro interface of Schrödinger suite[44,45].The vibrational frequency calculations were performed based on the minimum energy conformer derived from the gas-phase calculation at the DFT/B3LYP/6–311++G(d,p) level of theory using Gaussian09 [46]. The potential energy distribution (PED) calculation was carried out using the program MOLVIB-7.0 [47,48] and the PED of the title molecule was calculated as described earlier [49,50].

Results and discussion

Description of crystal structure

The title compound crystallized in non–centrosymmetric manner with space group $P2_1$ belonging to monoclinic crystal system. The crystal data and refinement parameters are summarized in Table 1. The hydrogen bonding interactions that stabilize the crystal structure are listed in Table 2. The ORTEP diagram of the title compound is shown in Fig.1. The title compound has a distorted H shaped folded molecular conformation. One side of the H shaped molecule consists of carboxylic acid and ethyl ester group and the other side has methoxy carbonyl and methylphenyl moiety. These two sides are interconnected by vinylamine group as illustrated in Fig. 1. The dihedral angle between the mean planes formed by atoms O1/O2/O4/C10-C14/O3 and O6/C1-C8/C15/C16 is 28.57(2)°. The maximum deviation is observed for the atom C14 [0.770 Å] from the former mean plane and the corresponding maximum deviation observed for the atom C8 is 0.705 Å from the latter mean plane. The dihedral angle between the bridged group (vinylamine) and the former mean plane is 17.05(2)°, whereas bridged group makes an angle of 44.80(2)° with the latter mean plane.

The crystal structure of the title compound is primarily stabilized by intramolecular N–H…O and O–H…O hydrogen bonds and intermolecular C–H…O and C–H…π interactions. The carboxylic acid moiety acts as a donor and as an acceptor for intramolecular N–H…O and O–

H…O hydrogen bonds and intermolecular C–H…O interactions. As shown in Fig. 2, the intramolecular N–H…O and O–H…O hydrogen bonds generate two fused pseudo six–membered rings namely *S*(6)–*S*(6) motifs [51]. The adjacent *S*(6)–*S*(6) motifs in the molecules are linked through an intermolecular C–H…O interaction which has a graph set motif of *C*(10) chain which runs parallel to the *c* axis (Fig. 2). Atom C16 acts as a donor and atom O2 of the carboxylic acid moiety acts as an acceptor for an intermolecular C16–H16A…O2 interaction. Atom C3 is involved in an intermolecular C–H…O interaction with atom O3 of carbonyl group of an adjacent molecule (Fig 3(a)). This interaction links the molecules into a *C*(5) chain which runs parallel to the *b* axis. These two intermolecular C–H…O interactions combine to form a R_4^4 (36) loop. As illustrated in Fig 3(a),there are four molecules located within this loop which are further stabilized by an intermolecular C–H...π interaction. Atom C7 participates in an intermolecular C–H…O interaction with atom O5 of carbonyl group (Fig 3(b)). This interaction interconnects the molecules in a *C*(5)chain fashion.

Hirshfeld surface analysis and PIXEL energy calculation

The Hirshfeld surface (HS) of the title compound was generated using Crystal Explorer [52]. The HS is used to identify the intermolecular interactions including H…H, O…H, C…H contacts. The contacts with distances equal to the sum of the van der Waals radii are indicated as white and the contacts with distances shorter than and longer than van der Waals radii are represented as red and blue, respectively. The decomposed two dimensional fingerprint plots (FP) quantify relative contributions of each of these intermolecular interactions involved in crystal packing. The FP is generated based on the d_e and d_i distances in which the former represents the distance from the HS to the nearest atom outside while the latter represents the distance from the HS to the nearest atom inside. Using Hirshfeld surface diagram (Fig 4), we have identified four intermolecular interactions (Table 2) that could possibly stabilize the crystal structure of the title compound. The intermolecular H…H contacts are predominant in the title compound and the relative contributions being 48%. The relative contributions for O…H/H…O and C…H/H…C contacts are 37% and 12.5% and the other contacts make only about 2.5% [(Fig 4(a) and Fig.5)].

The intermolecular interactions are further quantified by PIXEL method [33–35] which deals with the energy partitioned into dispersion, columbic, repulsion and polarization for each

pair of molecules that are interconnected by various intermolecular interactions. Before calculating the interaction energy, the distances involving hydrogen atoms were moved to their neutron values and electron density of the molecule has been obtained at MP2/6–31G** with the program Gaussian 09 [46]. The centroid distance between the pair of molecules which are held together by intermolecular interactions and various energy components of different molecular pairs are listed in Table 3. The interaction energy for the C7–H7A…O5 interaction being −10.4 kcal/mol and this interaction makes significant contribution to the crystal packing. The intermolecular interaction energy for the other C–H …O interactions are −6.1 and −3.2 kcal/mol. It is interesting to note that intermolecular C–H…π interaction contributes better to the crystal packing when compared with some of the intermolecular C–H…O interactions (Table 3). As mentioned earlier, the C–H…π interaction is formed in the tetrameric arrangement of the molecules which provides further stability.

Optimized structure

Selected geometric parameters derived from computational study are compared with those of parameters determined from X–ray crystallographic study. The comparative geometric parameters such as bond lengths, angles and torsion angles are listed in Table 4. The structural superimposition is carried out in order to compare the experimental structure with the structure obtained from the gas phase geometry optimization. The overall root mean square deviation (RMSD) involving non–hydrogen atoms for X–ray and optimized structures is 0.48 Å. The vinylamine group is found to be superimposed well compared to other regions of the molecule. The phenyl ring, ethyl ester and methoxy carbonyl groups are found to slightly away from the X–ray geometry (Fig 6). This might be a consequence of the molecular geometries derived from two different phases. In the isolated geometry optimization, intermolecular coulombic interaction with the neighboring molecule is absent, whereas intermolecular interactions are present in the crystalline state. As shown in Table 3, the largest deviations of bond lengths involving non–hydrogen atoms between experimental and theoretical calculation are for C1–C6 and C5–C6 (0.01 Å) and the highest deviations are observed for bond angles C1–C7–C8 (1.3°) and C7–C8–C15 (2.4°). These two bond angles are involving around C^{β} and C^{α} atoms of phenylalanine. The largest deviation is observed for the torsion angle C7–C8–N1–C9 [16.5°].

Analysis of polarizability and hyperpolarizability

Study of NLO property is gaining more attraction due to its wide range of application in the area of laser technology, optical communication and data storage technology. We have calculated the dipole moment (μ), polarizability and first order hyperpolarizability of the title compound using B3LYP/6-311++G(d,p) level of theory. Because the DFT method has been extensively used for organic NLO material to calculate polarizability and hyperpolarizability values. The values of the total electric dipole moment (μ), diagonal elements for the polarizability (α) tensor and total values for the first order hyperpolarizability (β) tensor are provided in Table 5. The calculated dipole moment is found to be 3.38075 D. The lowest absolute value of the dipole moment is found to be μ_y component. However, the absolute values of the dipole moments for components μ_x and μ_z are nearly the same, but in the opposite direction. The polarizability (α_{tot}) of the title compound is calculated and found to be 32.6384 x 10^{-24}e.s.u and anisotropy of the polarizability ($\Delta\alpha$) being 74.732 au. The calculated first hyperpolarizability (β_{tot}) of the title compound is found to be 63.3722x10^{-33} e.s.u. The intermolecular C–H…O and C–H…π interactions observed in the solid state of the title compound might be a key factor for the enhancement of the first order hyperpolarizability.

SHG activity

The nonlinear optical susceptibility of the title compound is examined using Kurtz and Perry method [53]. This method is an extremely good tool for initial screening of materials for SHG. The fundamental beam λ=1064 nm from Nd: YAG laser is used to test the SHG property. Pulse energy of 3 m J/ pulse, with 8 ns pulse width, repetition rate 10Hz and 90° geometry are used. Czeny–Turner monochromator is used to filter the fundamental beam. A photo multiplier tube (Hamamatsur 2059) is used as a detector. Powdered samples of the compound and standard KDP are used for experiment. The outcome of SHG signal with the energy 1.512 eV confirms the nonlinear optical activity of the title compound and the SHG efficiency is 8 fold excess that of the standard KDP (energy being 0.186 eV). Both experimental and theoretical calculations show that the title compound could act as a potential material for NLO applications.

Frontier molecular orbital and energy

The band gap energy is a critical parameter in determining the kinetic stability of the molecule. The highest occupied molecular orbital (HOMO) and lowest occupied molecular

orbital (LUMO) orbitals of the molecule are displayed in Fig 7. The band gap energy (HOMO–LUMO) clearly explains the charge transfer process within the molecule. The energy for HOMO and LUMO is calculated to be –6.67 eV and –1.44 eV, respectively. The band gap energy for the molecule is found to be 5.17 eV. This suggests that the title compound is kinetically highly stable molecule. The former and the latter orbitals exhibit electron donating and accepting characters, respectively. The HOMO is mainly located around atoms C8, N1, C9, C10, C12, O1, O2, O3 and O4; however the LUMO is mainly localized around N1, C9, C10, C11, C12, O3 and O1 atoms.

Mulliken atomic charges

The distribution of Mulliken atomic charges of the title molecule is shown in Fig 8. It is found that atoms C9, C11, C12 and C15 carbons are positively charged. The last three of atoms are attached to the oxygen atoms, while the C9 carbon atom is double bonded to vinylic carbon atom (C10). The remaining carbon atoms are negatively charged along with nitrogen and oxygen atoms. The highest atomic charges are observed for atoms H1N and H2O and both of these atoms are involved in hydrogen bonding interactions. The negatively charged lone pair O1, O3 and O5 oxygen atoms indicates that the charge is transferred from respective carbon atoms (C11, C12 and C15) to the attached lone pair oxygen atoms. The calculated Mulliken atomic charges are found to be 0.25203 e, –0.36187 e, 0.22767 e, –0.34758 e, 0.1418 e and –0.26696 e for atoms C11, O1, C12, O3, C15 and O5, respectively. Atoms C10 and C14 have more negative charge than other atoms which clearly indicates that the transfer of charge from C11 to C10 and H's to C14, respectively.

Molecular electrostatic potential map

The molecular electrostatic potential (MEP) map displays electrostatic potential regions of the molecules using simple colour coding. The MEP map for the title compound is shown in Fig.9. The MEP is used to determine the electrophilic and nucleophilic attacks during the reactions as well as hydrogen bonding interactions. The map is obtained at BL3YP/6-311G++(d,p) level of theory. Moreover, blue and red colours indicate the positive and negative potentials, respectively. The negative electrostatic potential is usually associated with the lone pair of electronegative atoms. The MEP map clearly indicates that the negative electrostatic

potentials localized on atoms O1, O3 to O6 and also seen for π electron cloud of the phenyl ring. The positive electrostatic potential sites are located around hydrogen atoms. These sites will provide information about where the intermolecular interactions take place.

Analysis of vibrational spectra

The title molecule consists of 42 atoms and having 120 normal modes of vibration. All vibrational modes of the title molecule are both IR and Raman active because the molecule possesses C_1 point group symmetry. The detailed vibrational assignments of fundamental modes of the title molecule along with the theoretical IR and Raman intensities and potential energy distributions are listed in Table. 6. The definition of internal coordinates of the title molecule is presented in the supplementary information section. The experimental and theoretical FT-IR and FT-Raman spectra are presented in Figs. 10 and 11.

N–H and O-H vibrations

The fundamental modes of vibrations for secondary amine N-H stretching and carboxylic acid O-H vibrations are normally occurring in the 3400-3250 and 3300-2500 cm^{-1}, respectively. The N-H stretching is calculated at 3230 with 85% PED and the O-H vibration is at 3208 with 86% PED. In the FT-IR spectrum, there is a peak observed at 3196 cm^{-1} and could be assigned for these vibrations. The in-plane and out-of-plane bending vibrations are listed in Table 6.

C-O and C=O vibrations

There are five C-O stretching vibrations possible for the title molecule of which four of them from ester groups and one from acid group. Interestingly, none of the C-O moieties from ester groups are involved in the intermolecular interactions. However, the C-O moiety of the carboxylic acid group is involved in the hydrogen bonding interaction. In alcohols, ethers, esters and carboxylic acids, the C-O bands are usually observed in the region 1320-1000 cm^{-1}. In the present study, the ester C-O bands are calculated at 1176, 1166, 1081 and 1057 cm^{-1} with more than 30% PED contributions. In the experimental FT-IR and FT-Raman spectra, six bands are seen in each of these spectra in the region 1300-1000 $cm^{-1}$and some of these bands can be assigned as C-O stretching vibrations. The C=O stretching vibrations of carboxylic acid and ester groups are observed at 1743 and 1700 cm^{-1} in FT-IR and at 1713 and 1702 cm^{-1} in FT-Raman

spectrum. The corresponding vibrations are calculated at 1724 and 1701 cm^{-1} with more than 50% PED contributions.

The C-H vibrations

The C-H stretching vibration of phenyl rings usually appear in the region 3000-3100 cm^{-1} [54]. For the title molecule, the phenyl ring C–H stretching vibrations are calculated at 3102, 3091, 3082, 3075 and 3063 $cm^{-1}$with each mode contributes about 99% of PED. The phenyl C-H stretching vibration of the title molecule is observed at 3061 cm^{-1} in the FT-Raman spectrum. The C-C-H in-plane bending vibrations of the phenyl ring are calculated at 1530, 1488, 1384, 1213 and 1188 with each mode contributes more than 50% of PED. The vinylic C-H stretching vibration is calculated at 3099 cm^{-1}. The C-H vibrations of the methyl and methylene groups of the title molecule are observed at 2984 and 2746 cm^{-1} in the FT-IR and in the region 2963-2725 cm^{-1} in the FT-Raman spectrum. It is of interest to note that the observed frequencies of 2746 and 2725 cm^{-1} are quite low for these vibrational modes and this might be a consequence of overtones. The calculated values for these vibrations are in the region 3075-2950 cm^{-1}. The C-H in-plane bending vibrations of the methyl groups are calculated at 1525 and 1530 cm^{-1} with 80% PED contributions.

The C-N vibrations

The C-N stretching vibration in the aliphatic amine group is usually observed in the region 1250–1020 cm^{-1}. In present investigation, the band observed at 1220 cm-1 in the FT-IR and at 1204 cm^{-1} in the FT-Raman could be assigned to C-N stretching vibration of the title molecule. The C-N stretching vibration is calculated at 1339 cm^{-1} with 31% of PED. The in-plane and out-of-plane bending C-N vibrations have also been identified and presented in Table 6.

The C-C vibrations

The C-C and C=C stretching vibrations are usually occurring in the region 1200-1650 cm^{-1} with variable intensity [55-60]. In the present study, the phenyl ring the C-C stretching vibrations are calculated at 1606 cm^{-1} with 55% of PED and at 1207 cm^{-1} with 38% of PED. The vinylic (C9=C10) vibration mode is calculated at 1625 cm^{-1} with 58% of PED. The observed frequencies of these vibrations are 1607, 1454 and 1275 cm^{-1} in the FT-IR and 1445 and 1256 cm^{-1} in the FT-Raman spectrum. The in-plane and out-of-plane bending C-C vibrations are presented in Table 6.

Conclusion

NLO active title compound is synthesized and characterized by experimental and theoretical studies. Crystal structure of the compound is stabilized by intramolecular N–H…O and O–H…O hydrogen bonds and intermolecular C–H…O and C–H…π interactions. The intermolecular interactions energies are calculated for the molecular pairs held together by various intermolecular interactions. We found that the intermolecular C7–H7A…O5 interaction contributes more to the crystal packing. It is of interest to note that the C–H…π intermolecular interaction contributed better compared to some of the C–H…O intermolecular interactions. Hirshfeld surface analysis suggests that the intermolecular H…H contacts are predominant (48 %). The band gap energy indicates that the title compound is kinetically stable. The MEP and Mulliken atomic charges are calculated using DFT method. The dipole moment, polarizability and first hyperpolarizability are also calculated from the optimized geometries. The title compound shows good SHG activity and found to show 8 fold excess that of the standard compound KDP. The complete vibrational assignments of the title molecule are proposed based on the observed and calculated FT-IR and FT-Raman spectrum.

Acknowledgements

The authors PV and AI thank the DST–India (FIST programme) for the use of Bruker SMART APEX-II diffractometer and the 400 MHz NMR facility at the School of Chemistry, Bharathidasan University. ST is highly grateful to the management of SASTRA University for their encouragement and financial support (Prof. TRR fund).

References

[1] P. Gunter, (Ed.), Nonlinear Optical Effects and Materials (2000) Springer.

[2] P.N. Prasad, D. J. Williams, Introduction to Nonlinear Optical Effects in Molecules and Polymers, Wiley (1991) New York.

[3] S. R. Marder, D. N. Beratan, L. T. Cheng, Science, 252(1991) 103–106.

[4] V. V. Nesterov, M.Y. Antipin, V. N. Nesterov, T. V. Timofeeva, J. Mol. Struct. 831 (2007) 18–25.

[5] P.S. Patil, K. Ramakrishna, H. K. Fun, R. S. Santhosh Kumar, D. Narayan Rao, J. Cryst. Growth. 303 (2007) 520–524.

[6] Y. Wang, D.F. Eaton, Chem. Phys. Lett. 120 (1985) 441–444.

[7] J. Zyss, I. Ledoux, Chem. Rev. 94 (1994) 77–105.

[8] M. Prakash, D. Geetha, M. L. Caroline, P.S. Ramesh, Spectrochimi. Acta A, 83 (2011) 461–466.

[9] M.L. Caroline, S.Vasudevan, Mater. Lett. 63 (2009) 41–44.

[10] M. Anbuchezhiyan, S. Ponuusamy, C. Muthamizgchelvan, Spectrochimi. Acta A, 74 (2009) 917–923.

[11] P.A. Cyrac, M. Vimalan, P. Sagayaraj, J. Madhavan, Physica B 405 (2010) 65–71.

[12] R. Mahalakshmi, S.X. Jesuraja, S.J. Das, Cryst. Res. Technol. 41 (2006) 780–783.

[13] N. Elleuch, A. B. Ahmed, H. Feki, Y. Abid, C. Minot, Spectrochimi. Acta A, 121 (2014) 129–138.

[14] T. Sujatha, P. A. Cyrac, M. Vimalan, J. M. Shyla, J. Madhavan, Physica B 405 (2010) 3365–3370.

[15] M.N. Bhat, S.M. Dharmaprakash, J. Cryst. Growth 236 (2002) 376–380.

[16] M. Prakash, D. Geetha, M. L. Caroline, Mater. Manuf. Process., 27 (2012) 519–522.

[17] R. Raju, C. Y. Panicker, P. S. Nayak, B. Narayana, B.K. Sarojini, C. Van Alsenoy, A. A. Al-Saadi, Spectrochimi. Acta A, 134 (2015) 63–72.

[18] M. Prakash, M. L. Caroline, D. Geetha, Spectrochimi. Acta A, 108 (2013) 32–37.

[19] S. Tamilselvan, M. Vimalan, I. Vetha Potheher, S. Rajasekar, R. Jeyasekaran, M. Antony Arockiaraj, J. Madhavan, Spectrochimi. Acta A, 114 (2013) 19–26.

[20] K. Govindarasu, E. Kavitha, Spectrochimi. Acta A, 133 (2014) 799–810.

[21] M. Prakash, D. Geetha, M. L. Caroline, Spectrochimi. Acta A, 81 (2011) 48–52.

[22] M. Amalanathan, I. Hubert Joe, V.K. Rastogi, J Mol. Struct., 1006(2011) 513–526.

[23] A. C.Peter, M. Vimalan, P. Sagayaraj, J. Madhavan, Physica B 405(2010) 65–71.

[24] T.G. Back,J.E. Wulff, Angew. Chem. Int. Ed.43 (2004)6493–6496.

[25] V. Iosub, A. R. Haberl, J. Leung, M. Tang, K. Vembaiyan, M. Parvez, T. G. Back, J. Org. Chem.75 (2010) 1612–1619.

[26] J. Baudoux, P. Lefebvre, R. Legay, M. C. Lasne, J. Rouden, Green Chem. 12(2010) 252–259.

[27] Y. Ryu, A. I. Scott, Tetrahedron Lett, 44 (2003) 7499–7502.

[28] A. Ilangovan, R. Ganesh Kumar, M. P. Kaushik, Synlett. 23 (2012) 2093–2097.

[29] J. J. McKinnon, D. Jayatilaka and M.A. Spackman, Chem. Commun.,(2007) 3814–3816.

[30] M.A. Spackman, D. Jayatilaka, CrystEngComm,11(2009) 19–32.

[31] M.A. Spackman, J.J. McKinnon, CrystEngComm, 4 (2002) 378–392.

[32] J.J. McKinnon, M.A. Spackman, A.S. Mitchell, Acta Cryst. B60(2004) 627–668.

[33] A. Gavezzotti, New J. Chem., 35 (2011) 1360–1368.

[34] A. Gavezzotti, J. Phys. Chem. B, 107 (2003)2344–2353.

[35] A. Gavezzotti, J. Phys. Chem. B, 106 (2002) 4145–4154.

[36] A. Altomare, G. Cascarano, C. Giacovazzo, A. Guagliardi, M.C. Burla, G. Polidori, M. Camalli, J. Appl. Cryst. 27(1994) 435–436.

[37] G. M. Sheldrick, Acta Cryst. A64(2008) 112–122.

[38] A. L.Spek, Acta Cryst. D65(2009) 148–155.

[39] C. F. Macrae, P. R. Edgington, P. McCabe, E. Pidcock, G.P. Shields, R. Taylor, M. Towler, J. van de Streek, J. Appl. Cryst. 39(2006) 453–457.

[40] Becke, A. D., J. Chem. Phys. 98(1993) 5648–5652.

[41] C. Lee, W. Yang, R.G. Parr, Phys. Rev. B 37 (1988)785–789.

[42] B. Miehlich, A. Savin, H. Stoll, H. Preuss, Chem. Phys. Lett. 157(1989) 200–206.

[43] A.D. Bochevarov, E. Harder, T. F. Hughes, J. R. Greenwood, D.A. Braden, D.M. Philipp, D. Rinaldo, M. D. Halls, J. Zhang, R.A. Friesner, Int. J. Quantum Chem., 113 (2013) 2110–2142.

[44] Schrödinger Release 2013–3: Jaguar, version 8.2, Schrödinger, LLC, New York, NY, (2013).

[45] Schrödinger Release 2013–3: Maestro, version 9.6, Schrödinger, LLC, New York, NY, (2013).

[46] M. J. Frisch, G. W. Trucks, H. B. Schlegel, G. E. Scuseria, M. A. Robb, J. R. Cheeseman, G. Scalmani, V. Barone, B. Mennucci, G. A. Petersson, H. Nakatsuji, M. Caricato, X. Li, H. P. Hratchian, A. F. Izmaylov, J. Bloino, G. Zheng, J. L. Sonnenberg, M. Hada, M. Ehara, K. Toyota, R. Fukuda, J. Hasegawa, M. Ishida, T. Nakajima, Y. Honda, O. Kitao, H. Nakai, T. Vreven, J. A. Montgomery, Jr., J. E. Peralta, F. Ogliaro, M. Bearpark, J. J. Heyd, E. Brothers, K. N. Kudin, V. N. Staroverov, T. Keith, R. Kobayashi, J. Normand, K. Raghavachari, A. Rendell, J. C. Burant, S. S. Iyengar, J. Tomasi, M. Cossi, N. Rega, J. M. Millam, M. Klene, J. E. Knox, J. B. Cross, V. Bakken, C. Adamo, J. Jaramillo, R. Gomperts, R. E. Stratmann, O. Yazyev, A. J. Austin, R. Cammi, C. Pomelli, J. W. Ochterski, R. L. Martin, K. Morokuma, V. G. Zakrzewski, G. A. Voth, P. Salvador, J. J. Dannenberg, S. Dapprich, A. D. Daniels, O. Farkas, J. B. Foresman, J. V. Ortiz, J. Cioslowski, and D. J. Fox. Gaussian 09, revision D.01; Gaussian, Inc., Wallingford, CT, (2013).

[47] T. Sundius, J. Mol. Struct. 218(1990) 321–326.

[48] T. Sundius, Vib. Spectrosc. 29(2002)89–95.

[49] J. Uma Maheshwari, S. Muthu, T. Sundius . Spectrochimi Acta A 123 (2014) 503-510.

[50] J. Uma Maheshwari, S. Muthu, T. Sundius . Spectrochimi Acta A 137 (2015) 841-855.

[51] J. Bernstein, R. E. Davis, L. Shimoni, N.L. Chang, Angew. Chem. Int. Ed. Engl. 34 (1995)1555–1573.

[52] S. K. Wolff, D. J. Grimwood, J. J. McKinnon, M. J. Turner, D. Jayatilaka and M. A. Spackman, CrystalExplorer (Version 3.0), University of Western Australia, (2012).

[53] S. K. Kurtz, T. T. Perry, J. Appl. Phys., 39 (1968) 3798.

[54] G. Varsanyi, Assignments for Vibrational Spectra of Seven Hundred Benzene Derivatives, Vol I, Adam Hilger, London, 1974.

[55] R. Wilfred Sugumar, Molecular and Atomic spectroscopy, MJP Publishers, Chennai, 2008.

[56] V. Krishnakumar, R. John Xavier, Indian J. Pure Appl. Phys. 41 (2003) 95–98.

[57] D.N. Sathyanarayana, Vibrational Spectroscopy Theory and Applications, second Ed., New Age International (P) Limited Publisher, New Delhi, 2004.

[58] N.P. Singh, R.A. Yadav, Ind. J. Phys. B 75 (4) (2001) 347–355.

[59] G. Varsanyi, Vibrational Spectra of Benzene Derivatives, Akademiai Kiado, Budapest, 1969.

[60] M. Silverstein, G.C. Basseler, C. Morill, Spectrometric Identification of Organic Compound, Wiley, New York, 1981.

Table 1. The crystal data and refinement parameters of the title compound.

Empirical formula	$C_{16}\ H_{19}\ N\ O_6$
Formula weight	320.31
T (K)	296(2)
Wavelength (Å)	0.71073
Crystal system	Monoclinic
Space group	$P2_1$
a (Å)	9.0961(3)
b (Å)	8.1789(3)
c (Å)	11.5679(4)
α (°)	90
β (°)	99.344(2)
γ (°)	90
V ($Å^3$)	849.19(5)
Z	2
Calculated density (Mg/m^3)	1.253
Absorption (mm^{-1})	0.097
F(0 0 0)	338
Crystal size (mm)	0.12 × 0.08 × 0.08
θ (°)	1.78– 26.50
Limiting indices	$-11 \leqslant h \leqslant 11, -10 \leqslant k \leqslant 10, -14 \leqslant l \leqslant 14$
Reflections collected/unique (R_{int})	8301/3002, (0.0220)
(θ °) Completeness (%)	(25.24), 99.9 %
Refinement method F^2	full-matrix least-squares on F^2
Data/restraints /parameters	3002/2/225
Goodness-of-fit(GOF) onF^2	1.039
Final R indices [I > 2σ(I)]	$R_1 = 0.0415$, $wR_2 = 0.1017$
R indices (all data)	$R_1 = 0.0603$, $wR_2 = 0.1130$
Largest difference in peak and hole (e A^{-3})	0.182 and -0.102

Table 2. Various intra- and intermolecular interaction observed in the title compound. The *Cg*1 is the centroid of the phenyl ring.

D—H···A	D—H	H...A	D···A	D—H···A	Label
O2—H2O···O3=C12	0.87(4)	0.87(4)	2.547(5)	145(5)	
N1—H1N...O1=C11	0.83(4)	2.04(4)	2.657(4)	131(3)	
C16-H16A...O2-C11	0.96	2.46	3.395(5)	165	1
C3–H3…O3=C12	0.93	2.64	3.469	149.02	2
C7–H7A…O5=C15	0.97	2.68	3.608	160.72	3
C8–H8…Cg1	0.97	2.803	3.611	152.30	4

Table. 3.PIXEL intermolecular interaction energies (kcal/mol) between molecular pairs related by a symmetry operation in the crystal

Centroid distance	E_{coul}	E_{pol}	E_{disp}	E_{rep}	E_{tot}	Symmetry	Important interactions
7.229	-5.7	-1.7	-6.4	3.4	-10.4	-x+1,y-1/2, z+2	C7–H7A…O5=C15
6.726	-2.4	-1.3	-10.9	6.5	-8.2	-x+2, y-1/2,-z+2	C8–H8…Cg1
9.330	-2.9	-0.7	-4.2	1.7	-6.1	-x+2, y-1/2,-z+3	C3–H3…O3=C12
11.568	-3.2	-0.7	-1.3	2	-3.2	x, y, z-1	C16-H16A...O2-C11

Table 4. Comparison of selected geometric parameters between X-ray and DFT calculation.

Bond length, Å		
Atoms	***X -Ray***	***DFT***
O6 C15	1.314(4)	1.345
O6 C16	1.441(4)	1.445
C8 N1	1.446(4)	1.449
C8 C15	1.503(4)	1.528
C8 C7	1.533(5)	1.559
C1 C2	1.386(4)	1.398
C1 C6	1.390(5)	1.400
C1 C7	1.503(4)	1.511
C9 N1	1.309(4)	1.328
C9 C10	1.378(4)	1.385
C15 O5	1.195(4)	1.203
C10 C11	1.444(6)	1.480
C10 C12	1.452(5)	1.457
O3 C12	1.227(4)	1.230
O4 C12	1.342(5)	1.350
O4 C13	1.452(5)	1.452
O2 C11	1.340(4)	1.335
O1 C11	1.215(5)	1.223
C2 C3	1.392(5)	1.394
C6 C5	1.383(5)	1.393
C4 C5	1.364(7)	1.395
C4 C3	1.365(7)	1.393
C13 C14	1.438(8)	1.520
Bond Angle, θ		
Atoms	***X -Ray***	***DFT***
C15 O6 C16	117.3(3)	116.0
N1 C8 C15	108.7(3)	109.5
N1 C8 C7	111.8(3)	112.3
C15 C8 C7	112.1(3)	108.9
C2 C1 C6	118.1(3)	118.6
C2 C1 C7	121.2(3)	121.0
C6 C1 C7	120.3(3)	120.4
N1 C9 C10	126.4(3)	126.0
C9 N1 C8	124.3(3)	123.9
O5 C15 O6	123.8(3)	124.6
O5 C15 C8	124.2(3)	124.7
O6 C15 C8	112.0(3)	110.6
C9 C10 C11	119.6(3)	119.9
C9 C10 C12	119.3(3)	119.5
C11 C10 C12	121.1(3)	120.6
C1 C7 C8	110.6(3)	113.0
C12 O4 C13	118.0(3)	117.4
C1 C2 C3	119.5(4)	120.7
C5 C6 C1	121.6(4)	120.9
O1 C11 O2	119.8(4)	120.1

Bond Angle, θ		
Atoms	***X -Ray***	***DFT***
O1 C11 C10	123.7(3)	121.9
O2 C11 C10	116.5(4)	118.0
C5 C4 C3	119.8(4)	119.7
O3 C12 O4	122.1(4)	121.5
O3 C12 C10	122.9(4)	124.0
O4 C12 C10	115.0(3)	114.4
C4 C5 C6	119.6(4)	120.1
C4 C3 C2	121.4(4)	120.0
C14 C13 O4	110.4(5)	111.6
Torsion angle , θ		
Atoms	***X -Ray***	***DFT***
C10 C9 N1 C8	-171.4(3)	-175.5
C15 C8 N1 C9	-147.8(3)	-134.6
C7 C8 N1 C9	87.8(4)	104.3
C16 O6 C15 O5	4.9(7)	-0.9
C16 O6 C15 C8	-175.9(4)	177.0
N1 C8 C15 O5	-15.6(5)	-27.38
C7 C8 C15 O5	108.5(4)	95.3
N1 C8 C15 O6	165.2(3)	154.4
C7 C8 C15 O6	-70.7(4)	-82.5
N1 C9 C10 C11	1.8(5)	2.8
N1 C9 C10 C12	179.6(3)	-178.5
C2 C1 C7 C8	96.1(4)	95.0
C6 C1 C7 C8	-77.4(4)	-84.0
N1 C8 C7 C1	-58.2(4)	-64.4
C15 C8 C7 C1	179.4(3)	174.2
C6 C1 C2 C3	1.9(5)	0.1
C7 C1 C2 C3	-171.7(3)	-179.0
C2 C1 C6 C5	-1.3(5)	-0.1
C7 C1 C6 C5	172.4(3)	179.0
C9 C10 C11 O1	-2.6(7)	-1.1
C12 C10 C11 O1	179.9(5)	-179.7
C9 C10 C11 O2	177.9(4)	178.5
C12 C10 C11 O2	0.4(6)	-0.1
C13 O4 C12 O3	4.8(7)	1.3
C13 O4 C12 C10	-176.5(4)	-179.0
C9 C10 C12 O3	-177.6(4)	-178.8
C11 C10 C12 O3	-0.1(6)	-0.2
C9 C10 C12 O4	3.8(6)	1.5
C11 C10 C12 O4	-178.7(4)	-179.8
C3 C4 C5 C6	0.3(7)	0.1
C1 C6 C5 C4	0.1(6)	0.0
C5 C4 C3 C2	0.4(7)	-0.1
C1 C2 C3 C4	-1.6(6)	0.0
C12 O4 C13 C14	89.4(6)	85.7

Table5.The values of calculated dipole moment (μ), polarizability (α), first order hyperpolarizability (βtot) components of the title compound.

Polarizability α		First order hyperpolarizability β	
α_{xx}	228.984	β_{xxx}	-2.85115528E+01
α_{xy}	6.782	β_{yyy}	1.17386004E+02
α_{xz}	15.165	β_{zzz}	1.20986218E+02
α_{yy}	173.380	β_{xyy}	7.67927305E+01
α_{zy}	11.207	β_{xzz}	1.62619201E+02
α_{zz}	258.332	β_{yxx}	3.91923070E+01
<α>	220.232	β_{yzz}	1.29510570E+02
α_{total}	32.6384 x 10^{-24}e.s.u	β_{zxx}	7.99751969E+01
Δα(au)	74.732	β_{zyy}	1.50739805E+02
Dipole moment, μ (D)		β_{xyz}	1.88213569E+02
μ_x	2.49703	β_{tot} (au)	7.45249988E+01
μ_y	0.48142	β_{tot} (e.s.u)	63.3722x10^{-33}e.s.u
μ_z	-2.22766		
μ	3.38075		

Table 6. Tentative vibrational assignments for the title molecule.

S. No.	Observed frequencies		Calculated frequencies		IR intensity	Raman activity	Vibrational assignments (PED %)
	FTIR	Raman	Unscaled	Scaled			
1			3383	3230	330.14	19.89	υNH (85) + υOH (14)
2	3196		3361	3208	274.32	108.10	υOH (86) + υNH (14)
3			3191	3102	10.64	251.26	υCHR (99)
4			3189	3099	1.57	28.64	υCH (98)
5			3181	3091	20.39	38.18	υCHR (99)
6			3172	3082	6.09	98.14	υCHR (99)
7			3165	3075	10.38	75.87	υCH (99)
8			3164	3075	0.99	39.29	υCHR (99)
9		3061	3152	3063	7.11	47.55	υCHR (99)
10		2963	3133	3044	18.32	10.81	υCH (100)
11			3132	3043	14.17	50.45	υCH (100)
12			3111	3022	9.32	75.19	υCH (100)
13			3097	3009	32.08	100.38	υCH (100)
14			3094	3006	14.06	42.09	υCH (100)
15			3080	2992	0.96	42.69	υCH (100)
16			3073	2987	25.34	117.62	υCH (100)
17	2984		3056	2971	31.53	165.93	υCH (100)
18			3043	2957	17.41	139.07	υCH (100)
19		2933	3035	2950	16.89	186.31	υCH (100)
20	1743	1713	1806	1724	236.98	9.30	υC=O (86)
21	1700	1702	1749	1701	572.80	13.15	υC=O (50) + βHOC (17) + υC=C (10)
22			1683	1638	24.08	81.61	υCN (27)+βCNH(21)+υC=C(18)+υC=O(11)+βNCH(10)
23			1659	1625	837.65	43.90	υCCR (58)+ βCCHR (27)

24	1607	1604	1643	1606	23.30	31.34	υC=O (55) + υCC (55)
25			1623	1605	0.76	8.49	βCCR (48) + βCCHR (20) + υC=O (15)
26			1526	1530	9.65	0.69	βCCHR (63) + υCCR (26)
27			1506	1530	29.14	1.76	βHCH (80)
28			1497	1525	10.47	6.79	βHCH (80) + βOCH (19)
29			1493	1517	47.65	22.23	βHCH (77) + βCCH (10)
30			1490	1513	7.36	4.63	βHCH (73) + βCCH (18)
31			1486	1510	34.52	9.38	βHCH (92)
32			1484	1508	11.56	12.00	βHCH (88)
33			1483	1500	6.27	0.86	βCCC (50) + βHCH (42)
34			1477	1489	193.46	6.08	βHOC (49) + υCO (16)
35			1470	1488	45.78	2.77	βCCHR (56) + υCCR (27)
36			1445	1445	247.01	19.42	βCCH (24) + βNCH (20) + υCO(13) + βOCH (12)
37	1454	1445	1423	1444	45.35	4.38	βCCH (31) + βOCH (22) + βNCH (13) + βHCH (10)
38			1405	1425	99.53	11.62	βCCH (47) + βHCH (38) + βOCH (10)
39	1400		1393	1388	37.41	12.34	υCC (30) + βCCH (18) + βCCC (12)
40	1379		1371	1384	35.31	8.72	βCCHR (52) + βCCH (22) + υCC (13)
41			1363	1370	27.50	4.12	βCCH (52) + υCC (14) + βCCHR (13)
42			1356	1361	120.38	25.88	βOCH (50) + βCCH (40)
43			1349	1354	10.79	22.13	βCCH (30) + υCC (26) + βCNH (10)
44	1339		1337	1339	23.35	9.45	υCN (31) + βCCH (18), βNCH (10)
45			1331	1314	8.06	5.43	υCCR (33) +βCCH (29) + βCCHR (12) + υCN (11)
46			1304	1305	195.40	12.10	βCCH (43) + υCCR (33)
47	1275	1256	1295	1283	412.15	20.31	υCC (33) + υCO (20)
48	1220		1231	1233	71.55	7.89	βOCH (73) + βHCH (11)
49			1223	1228	0.99	21.73	βCCH (38) + υCCR (15)
50			1216	1213	37.03	13.28	βCCHR (61) + υCCR (17) + υCC (14)
51			1211	1211	105.16	1.63	βCCH (48) + βOCH (26)
52			1204	1207	2.72	3.22	υCC (38) + υCCR (23) + βCCHR (23)
53		1204	1193	1200	35.00	5.36	βOCH (90)

54			1185	1188	211.63	4.73	βCCHR (56) + υCCR (37)
55			1182	1176	65.58	3.92	υCO (57) + υCC (18)
56			1171	1166	1.88	1.98	υCO (47) + βCCH (16)
57	1183		1123	1118	170.52	3.41	βCCH (55) + υCC (18) + βCCO (11)
58			1115	1109	83.62	2.27	υCCR (30) + βCCHR (24) + υCN (12) + υCO (10) + βCCH (10)
59	1088	1112	1101	1081	108.50	0.68	υCO (30) + υCN (19)
60			1087	1057	33.53	11.19	υCO (35) + υCN (19) + υCC (15)
61		1031	1049	1043	3.12	14.60	υCCR (47) + βCCCR (26) + βCCHR (25)
62			1024	1016	10.54	8.32	υCCR (50) + βCCCR (30)
63			1018	1013	0.03	30.21	γNC (44) + τCN (19) + υCC (10) + τCC (10)
64	1000	1002	1013	1001	14.22	11.57	γCH (51) + τCCR (15)
65			1007	997	13.69	6.72	γCH (26) + υCC (22)
66			1005	984	15.56	19.38	υCC (48) + υCO (25)
67			999	981	7.78	1.32	γCH (74) + τCCR (23)
68			988	973	0.16	0.06	υCC (44) + υCO (28)
69			950	934	3.92	21.74	γCH (37) + υCO (34)
70	912		926	914	7.65	14.61	υCO (37) + γCH (30)
71			884	880	7.91	4.60	βCCH (28) + υCC (26) + υCO (10)
72	870	861	872	864	1.47	10.96	βCCH (35) + υCO (29) + βCOC (14)
73			859	854	0.82	0.29	γCH (78) + τCCR (19)
74			853	844	3.53	10.63	υCO (38) + υCC (23) + βCCH (18)
75			842	835	12.49	1.48	υCC (27) + υCCR (14) + υCO (11)
76			835	829	74.08	1.63	γNC (44) + τCN (20) + γCC (15)
77	813	815	821	816	99.15	0.37	τCO (91)
78			809	812	8.55	5.40	βCCH (35) + υCO (16) + υCC (15)
79			786	781	8.58	0.09	γCC (82)
80	771		773	771	29.64	0.72	γCH (37) + γCC (19)
81			758	764	3.89	3.91	υCO (18) + βCCH (18) + βOCO (14) + βCOC (10) + βCCO (10)
82		744	749	751	3.20	7.96	υCC (15) + βOCO (12) + υCO (10)

83			739	734	2.12	0.17	γCC (78) + τCO (14)
84			724	721	15.74	6.80	γOC (36) + γCH (16) + υCC (15)
85	710		713	710	38.51	0.48	γCH (54) + τCCR (29) + γCC (10)
86			643	652	5.28	2.76	βOCO (24) + βCCO (24) + βCCC (17)
87			634	641	0.15	3.40	βCCCR (64) + βCCHR (26)
88	634		579	583	5.36	0.57	βCCCR (21) + βCCC (14)
89			541	544	11.77	0.78	βNCC (19) + υCC (17) + βCCH (11) + βCCCR (11) + βCCO (11)
90	504		502	502	29.26	2.33	γCC (27) + τCCR (13) + υCC (12)
91			464	472	6.84	1.19	βCCO (48) + βCCH (17) + υCC (11) + βCOC (10)
92			453	460	0.70	1.71	βCCO (61) + υCC (16)
93			421	423	2.98	0.93	βNCC (15) + βCCC (12) + υCC (12) + βCCO (12)
94			415	413	0.07	0.04	τCCR (64) + γCH (28)
95			406	411	2.02	1.36	βNCC (20) + βCCO (19) + βCCC (16)
96		392	391	389	6.18	1.84	γCC (32) + τCC (30) + τCN (13)
97			373	377	32.07	0.39	βCOC (25) + τCC (18) + βCCO (15) + βCCC (13)
98			342	345	3.40	0.98	βCCC (35) + τCC (18)
99			338	341	1.80	0.79	βCCC (23) + βCCO (20) + βCOC (10)
100			315	319	28.15	4.36	βCOC (43) + βCCC (11)
101		293	293	294	14.22	0.95	βCOC (15) + τCC (14) + υCC (13) + βCCC (12) + βNCC (10)
102			258	258	0.43	2.25	τCC (19) + βCCC (16) + τCCR (14) + υCC (10)
103		229	230	229	3.04	2.72	τCC (32) + τCO (19) + βCCC (17) + υCC (14)
104			206	207	0.94	0.93	βCCO (16) + τCC (15) + βCCC (11) + τCO (10)
105			200	201	2.60	0.47	τCC (37) + τCO (22) + βCOC (12)
106			190	189	4.59	1.24	τCC (35) + γCC (26) + τCO (14)
107			160	161	1.37	0.68	τCO (33) + βCCO (12) + βCCC (11) + τCC (10)
108			129	129	0.31	0.23	τCO (63) + τCC (13)
109			125	124	1.07	0.43	τCC (50) + τCO (43)
110			115	115	0.16	2.45	τCO (37) + τCC (23)
111			95	94	1.18	0.71	τCC (50) + τCO (28)
112			85	86	0.96	0.89	τCC (29) + τCO (15) + βCCC (14) + βNCC (13)

113	66	66	66	0.70	0.91	τCO (45) + γCC (13) + βCCC (11)
114		63	63	0.24	1.05	τCC (49) + τCO (20)
115		55	54	0.06	1.58	τCC (32) + τCO (24)
116		42	42	0.83	2.05	τCC (59) + τCO (20)
117		33	33	0.48	2.34	τCC (67) + γNC (11)
118		28	28	0.78	1.00	τCC (77)
119		16	17	0.24	2.44	τCC(54) + γNC (18) + τCN (16)
120		10	10	1.51	1.95	τNC (67) + τCCC (18)

υ-stretching;β,in-plane bending;γ-out-of-plane bending; τ, torsion

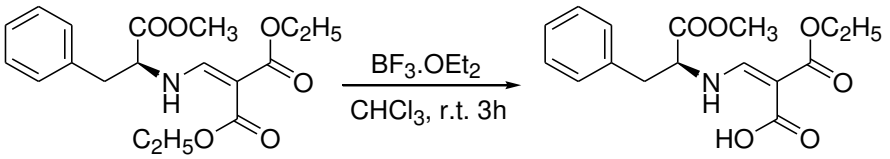

Scheme 1. (2E)-2-(ethoxycarbonyl)-3-[(1-methoxy-1-oxo-3-phenylpropan-2-yl)amino] prop-2-enoic acid

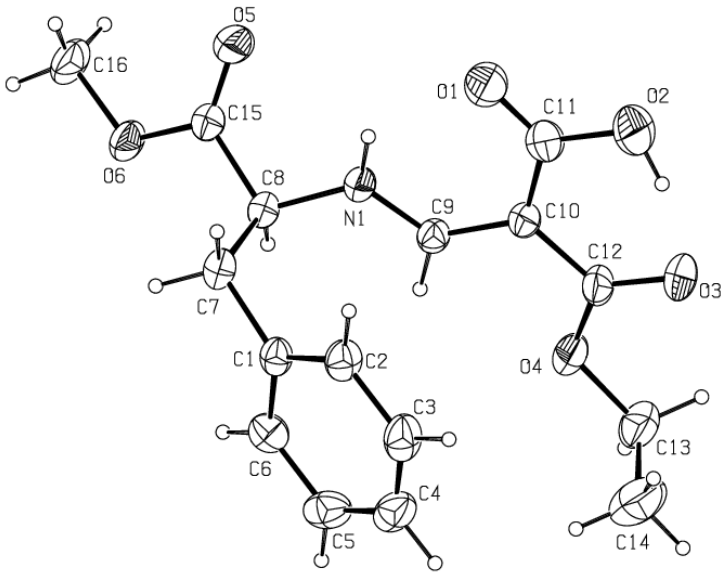

Fig. 1

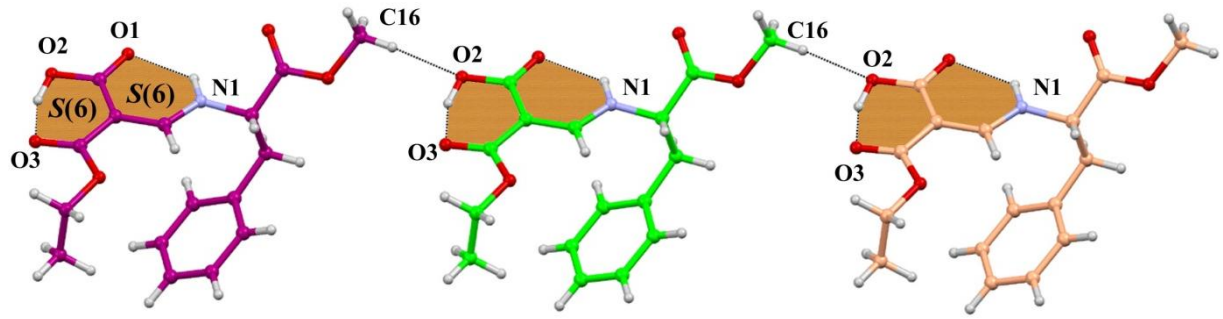

Fig. 2

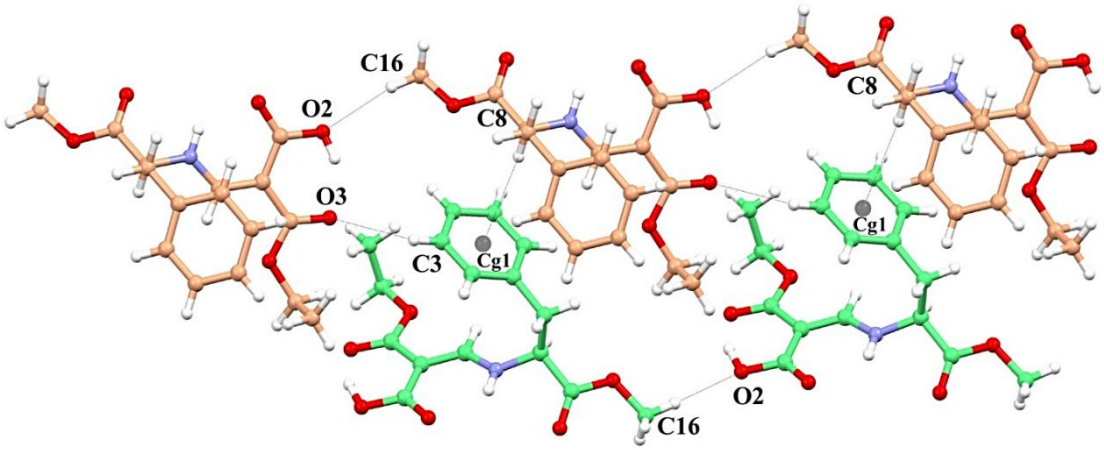

Fig. 3(a)

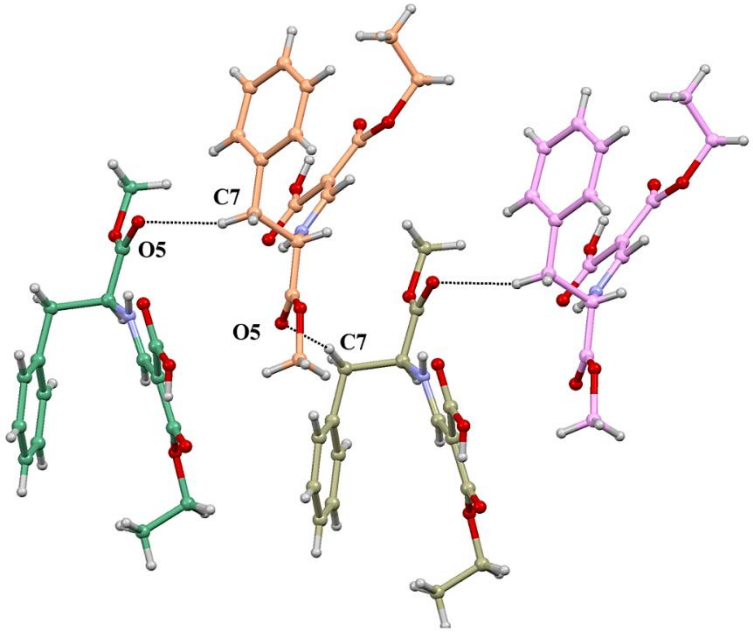

Fig. 3(b)

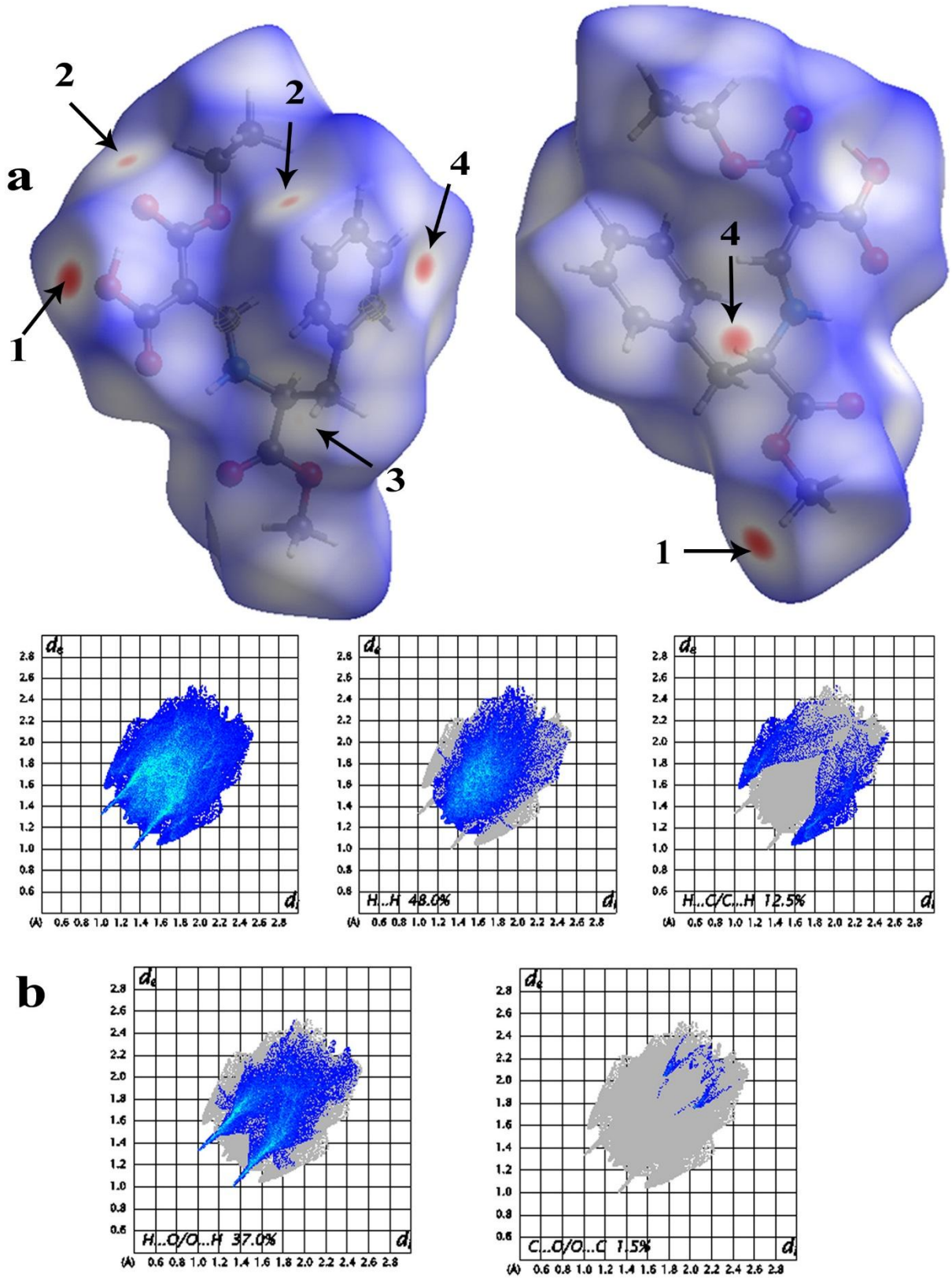

Fig. 4

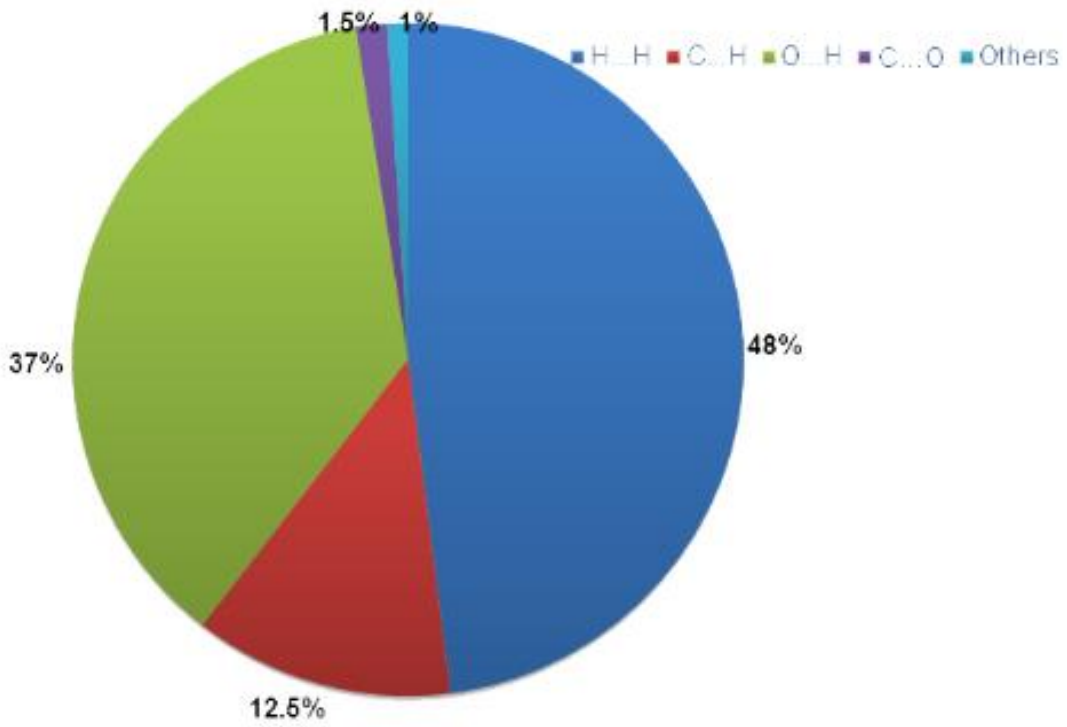

Fig. 5

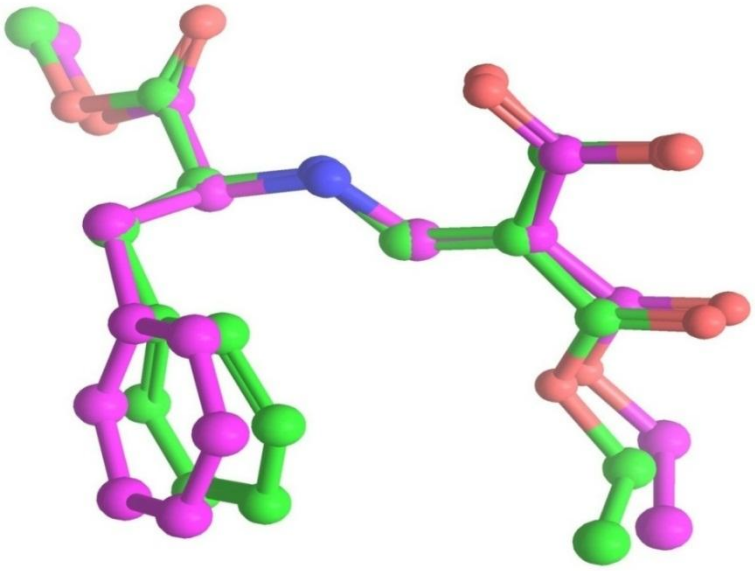

Fig. 6

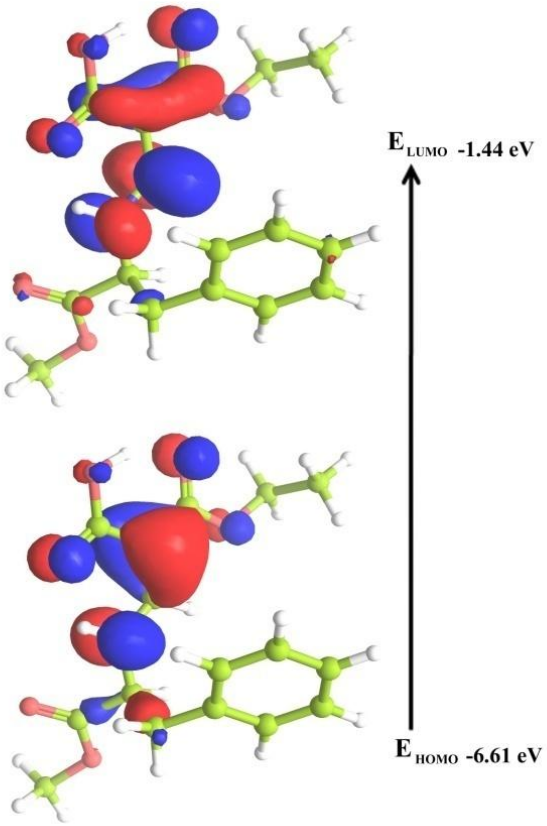

Fig. 7

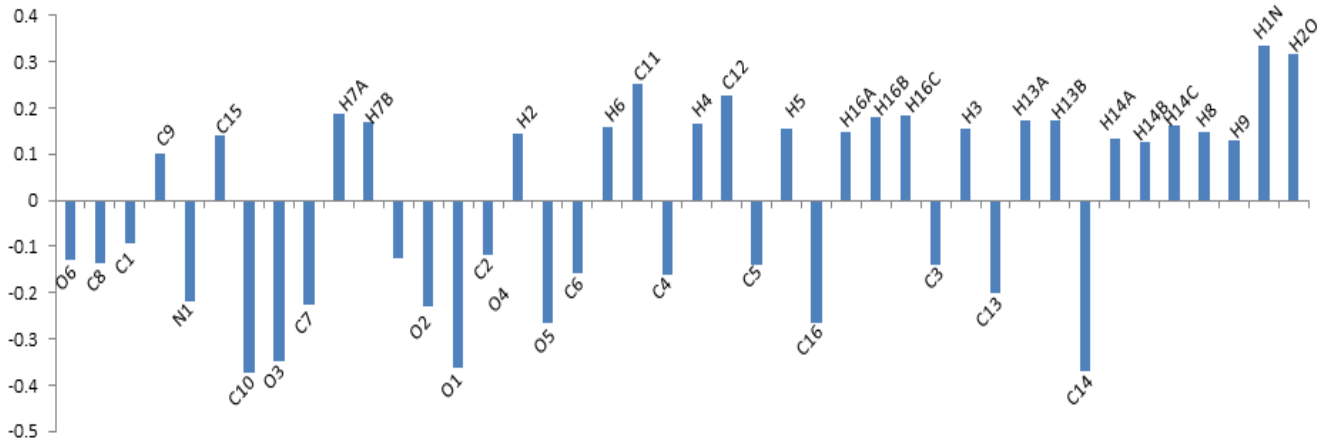
0.4
0.3
0.2
0.1
0
-0.1
-0.2
-0.3
-0.4
-0.5
O6
C8
C1
C9
N1
C15
C10
O3
C7
H7A
H7B
O2
O1
C2
O4
H2
O5
C6
H6
C11
C4
H4
C12
C5
H5
C16
H16A
H16B
H16C
C3
H3
C13
H13A
H13B
C14
H14A
H14B
H14C
H8
H9
H1N
H2O

Fig. 8

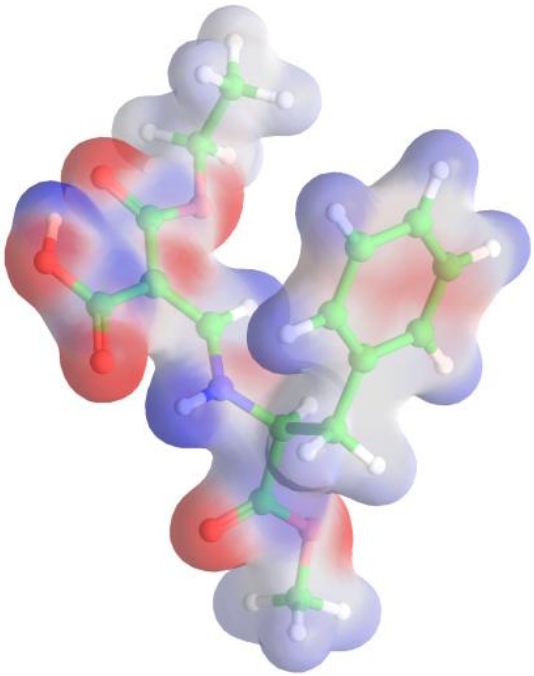

Fig. 9

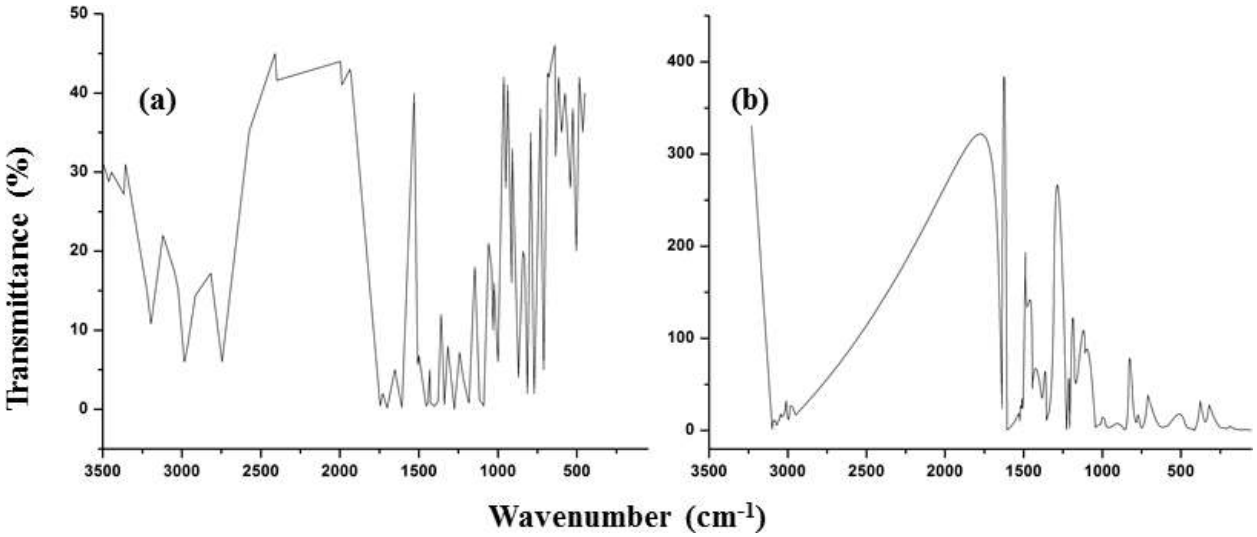
(a)
(b)
Transmittance (%)
Wavenumber (cm-1)

Fig. 10

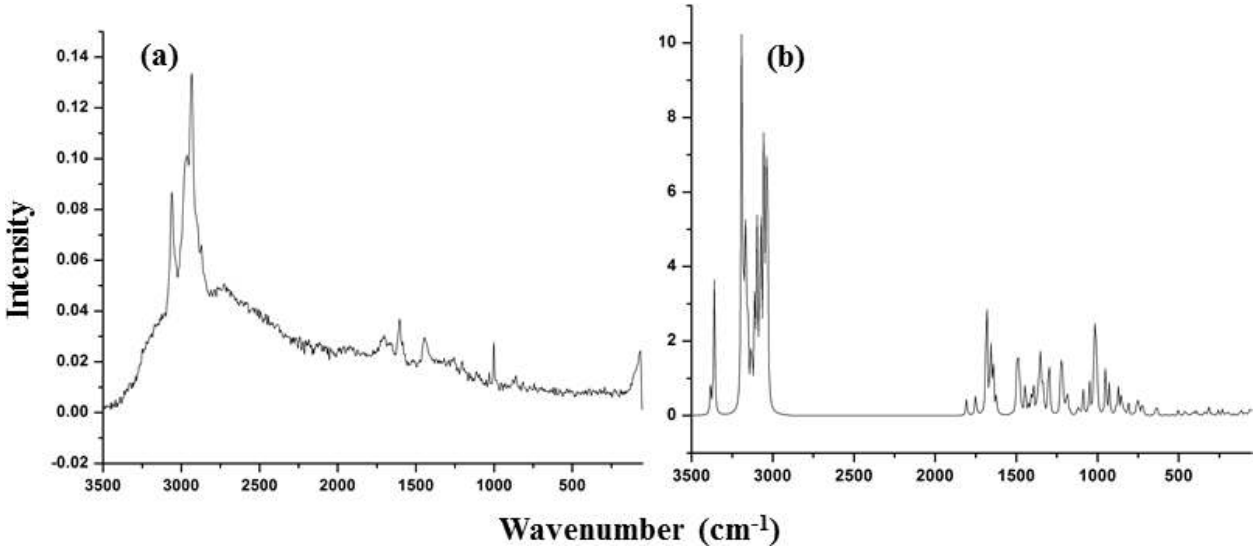
(a)
(b)
Intensity
Wavenumber (cm-1)

Fig. 11

Figure legend:

Fig. 1. Perspective view of the title compound showing the distorted H shaped conformation with atom numbering scheme.

Fig.2. Molecules comprising pseudo six membered rings are interconnected by an intermolecular C–H…O interaction.

Fig. 3(a) Part of the crystal structure showing the formation of tetrameric molecular arrangement. The combinations two intermolecular C–H…O interactions generate $R_4^4(36)$ loop. The ring centroid positions are represented as spheres. (b) Part of the crystal structure showing an intermolecular C–H…O interaction links the molecules into a $C(5)$ chain motif.

Fig. 4(a) Two different orientations of Hirshfeld surface mapped with d_{norm} and potential intermolecular contacts are labelled 4(b) Two dimensional fingerprint plots for the title compound. Various reciprocal close contacts and their contributions are indicated.

Fig. 5. Pie diagram showing the relative contributions of various intermolecular contacts.

Fig.6. Structural superimposition of experimental (green) and theoretical (magenta) structures involving only non-hydrogen atoms.

Fig. 7. HOMO and LUMO orbitals of the title compound.

Fig.8. The Mulliken atomic charge distributions of the title compound.

Fig.9. Molecular electrostatic potential map for the title compound.

Fig. 10. FT-IR spectra of the title molecule (a) Experimental (b) B3LYP/6-311G++(d,p).

Fig. 11. FT-Raman spectra of the title molecule (a) Experimental (b) B3LYP/6-311G++(d,p).

Supplementary Material

Click here to download Supplementary Material: Supplementary information_revised.docx